Journal of
Materials Chemistry A

Accepted Manuscript

This is an *Accepted Manuscript*, which has been through the RSC Publishing peer review process and has been accepted for publication.

Accepted Manuscripts are published online shortly after acceptance, which is prior to technical editing, formatting and proof reading. This free service from RSC Publishing allows authors to make their results available to the community, in citable form, before publication of the edited article. This *Accepted Manuscript* will be replaced by the edited and formatted *Advance Article* as soon as this is available.

To cite this manuscript please use its permanent Digital Object Identifier (DOI®), which is identical for all formats of publication.

More information about *Accepted Manuscripts* can be found in the **Information for Authors**.

Please note that technical editing may introduce minor changes to the text and/or graphics contained in the manuscript submitted by the author(s) which may alter content, and that the standard **Terms & Conditions** and the **ethical guidelines** that apply to the journal are still applicable. In no event shall the RSC be held responsible for any errors or omissions in these *Accepted Manuscript* manuscripts or any consequences arising from the use of any information contained in them.

Journal of Materials Chemistry A

Dynamic Article Links ►

Cite this: DOI: 10.1039/c0xx00000x

PAPER

www.rsc.org/xxxxxx

The composite electrode of $LiFePO_4$ cathode materials modified with exfoliated graphene from expanded graphite for high power Li-ion Batteries.

Tiefeng Liu, Li Zhao, Junsheng Zhu, Bo Wang and Chenfeng Guo, Dianlong Wang☆

Received (in XXX, XXX) Xth XXXXXXXXX 20XX, Accepted Xth XXXXXXXXX 20XX
DOI: 10.1039/b000000x

Recent years, the copious papers have reported the fruitful modifications for $LiFePO_4$-based composites and exhibited excellent electrochemical performance in term of rate capability and cycling stability. Besides, the optimizations of bulk electrode are essential to keep pace with composites by enhancement of electronic and ionic transport to further improve the power performance of electrode. Therefore, in this work, a facile strategy is adopted to fabricate the composite electrode with the NMP solvent containing large-size multilayer graphene, which is prepared by exfoliation of economical expanded graphite under high power ultrasound in the isopropyl alcohol. Active $LiFePO_4$ nanograins as well as conductive additives are attached to the superior conductive graphene and thereby the fast pathways are established as a "highway" for electronic transport in bulk electrode. As a result, this composite electrode exhibits a lower polarization at the high-rate charge/discharge process. The operating flat voltage of 20*C* rate is maintained more than 3.0 V in one minute and its discharge capacity is up to 107.8 $mAh \cdot g^{-1}$, representing a better energy density and power density.

Introduction

Due to the worry about the energy shortage and air pollution, the electric vehicles (EVs) and hybrid electric vehicles (HEVs) are proposed to alleviate the consumption of fossil fuel and decrease exhaust emissions because of the electric energy is abundant and efficient. As for the key of EVs and HEVs, lithium-ion batteries (LIBs) are the most promising candidates due to light weight and high energy density. Compared with other cathode materials, $LiFePO_4$ has attracted much attention owning to relatively high capacity of 170 $mAhg^{-1}$, environmental benignity, low cost and especially superior safety.[1-2] However, its power performance is restricted by the drawbacks of sluggish lithium ion diffusion and poor electronic conductivity,[3-5] which are the major obstacles limiting the widespread application in LIBs. Herein, the extensive attempts have been performed to improve the ionic and electronic conductivities, including electronically conductive coating and structural doping.[6-13] In particular, the amorphous carbon coatings derived from organics pyrolysis are the most efficient strategy to enhance electrical conductivity. Meanwhile, the in-situ modifications of carbon coatings on the particles also restrict the crystal growth and suppress agglomeration. The reduction of particle size lessens the distance of Li ion diffusion in the crystal.[14-17] Recently, the in-situ graphene-modified $LiFePO_4$ is frequently reported due to the improved electrochemical performance arising from superior electrical conductivity and high specific surface area of graphene.[18-33] Normally, reduced graphene oxide (RGO) is often adopted due to its low cost and good dispersion in various solvents.[19-29] In contrast, the high-quality graphene is prepared via chemical vapor deposition (CVD) and epitaxial growth,[32-36] which are seldom used as the preferred choice because of its high material cost, low yields and the difficulties associated with dispersion in aqueous solution. Nevertheless, many defects and organic functional groups of RGO weaken its superior conductivity.[37] Moreover, some reducing agents for RGO, which are toxic and dangerous, threaten environmental safety. Therefore, the proper choice of graphene as additives for $LiFePO_4$ remains a great challenge involved with the economical cost and simple synthetic processes.

In sum, the fruitful modifications of $LiFePO_4$ make it possible to achieve high power batteries. In addition to the ongoing optimization of $LiFePO_4$-based composites, the modifications of bulk electrode are also crucial to enhance the electronic and ionic transport. Singh et al.[38] reported the $LiFePO_4$-based electrodes were fabricated by hydrogen carbonate salt templates creating 3D highly inter-connected ionic pathways and exhibited high performance. On the other hand, fast electronic transport from the current collector to outer active materials need to be established with the essential modification for bulk electrode. The new obstacles of the electronic transport will probably occur inside bulk electrode due to the insulated PVdF binder and the electronic migration through the intimate contact among the particles. These bottlenecks indicate that there is a large room for

reducing internal resistance and increasing the efficiency while reducing the energy consumption arising from the polarization.

In this article, a facile method is designed to add the graphene into $LiFePO_4$-based electrode for enhancement of electronic transport. The worm-like expanded graphite is easily obtained through abrupt thermal treatment of economical expandable graphite. Multilayer graphene is prepared by ultrasonic exfoliation of expanded graphite in the isopropyl alcohol and then with pure treatment of HNO_3. Subsequently, based on the previous papers, multilayer graphene is easily prepared or dispersed with sonication in the oil solvent, such as NMP[34, 39, 40] and DMF[29, 41-44]. Fortunately, the NMP solvent also is used to ensure mixing the active materials, conductive additives and the binder of PVdF evenly. Hence, the hydrophobic multilayer graphene is easily added into the slurry to fabricate the composite electrode due to the NMP solvent containing low concentration of graphene. The large-size multilayer graphene sheets are embedded inside bulk electrode as a "highway" for electronic transport for rapid charge/discharge process. As a result, the composite electrode exhibits a lower polarization at the high-rate charge/ discharge process. At 1*C* rate, the higher operating flat voltage of nearly 3.4 V is maintained and the distance between the charge/discharge potential is only 0.46 V. At the high rate of 20*C*, the power performance is achieved by the high operating flat voltage, more than 3.0 V in short moment, and the discharge capacity of up to 107.8mAh·g^{-1}.

Experiment

The preparation of multilayer graphene

The worm-like expanded graphite (denoted EG) was prepared via rapid heat-treatment for expandable graphite and then sonicated in the isopropyl alcohol (denoted IPA). After filtering the IPA, dark gray multilayer graphene (denoted MG-IPA) was obtained. Subsequently, the MG-IPA was dispersed in 65 wt.% HNO_3 under sonication (**Be careful**) in order to remove the impurities on the multilayer graphene sheets. The MG-HNO_3 was obtained by filtering the HNO_3. The MG-HNO_3 was annealed under 300 ^oC in Ar atmosphere to remove residual water and HNO_3. Finally, the proper amount of MG was added into the NMP solvent and sonicated for one hour to achieve the homogeneous liquid with a certain concentration. The synthetic route of the clean MG sheets is displayed in Scheme 1.

The preparation of composite electrode

The carbon-coated $LiFePO_4$ nanocomposites (C-LFP) were synthesized as our previous report.[45, 46] The active materials (80 wt.%), acetylene black (10 wt.%), and a polyvinylidene fluoride (PVDF) binder (9 wt.%) were dispersed in Nmethylpyrrolidone (NMP) solvent containing MG (1 wt.%) to form a homogeneous slurry. The obtained slurry was pasted on an Al foil and then dried at 100 °C over night in a vacuum oven to remove NMP solvent. The composite electrode was fabricated by cutting round disks of 14 mm in diameter as the working electrode in the electrochemical test, which is denoted as C-LFP/MG. For comparison, a common electrode was fabricated as the same way without MG, replaced with 1 wt.% acetylene black (AB), which is denotes as C-LFP/AB.

Material characterizations

The morphology of the as-prepared samples was characterized by field-emission scanning electron microscopy (SU8000 Series), high resolution transmission electron microscopy (JEM-2100 and Fei Tecnai G20). Raman measurements were performed with a Jobin Yvon HR800 micro-Raman spectrometer at 457.9 nm.

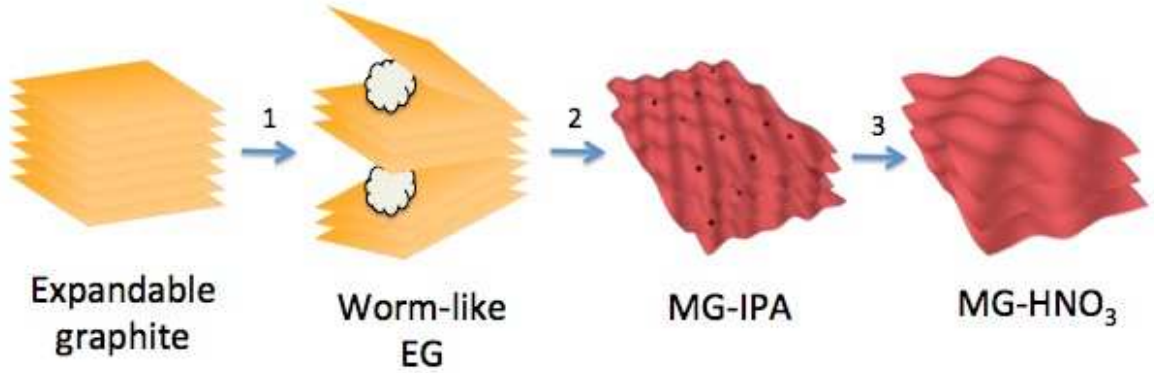

Scheme 1. Schematic procedures used to prepare MG. Step 1: Rapid heat-treatment at 800 ^oC in one minute; Step 2: The sonication in the IPA for one hour; Step 3: The sonication in 65 wt.% HNO_3 for one hour and the thermal treatment at 300 ^oC for one hour.

Electrochemical measurements

The electrochemical performances of electrodes were evaluated with using a CR2025 coin cell. The coin cell was assembled with a Li foil as the counter electrode, a polypropylene micro-porous film (Celgard 2400) as separator, and EC/DMC/DEC-based (1:1:1 by weight) electrolytes containing 1 M of $LiPF_6$ in a glove box filled with pure Ar. The charge–discharge tests were performed using Neware Battery Testing System at different rates with a voltage window of 2.5~4.2 V (*vs.* Li^+/Li). Electrochemical impedance spectroscopy (EIS) was investigated with CorrTest electrochemical workstation. Cyclic voltammograms (2.5~4.2 V, 0.1 mVs^{-1}) were performed on CHI 630B electrochemical workstation. All the tests were performed at room temperature.

Results and discussion

Characterizations

SEM and TEM are both essential tools to observe the morphology and microstructure of as-prepared samples in nano-scale. Due to thermal treatment causing the hasty decomposition of intercalation compounds, expandable graphite rapidly expands along c-axis, leading the formation of the worm-like structure

shown in Fig. 1a. At high magnifications, lots of translucent and wrinkled graphene and interspaces are observed on the surface of worm-like EG in Fig. 1b**.** Therefore, the interspaces among interlayers are easily embedded by small moleculars and thereby expanded graphite is exfoliated to graphene in the IPA under sonication (Fig. 1c and Fig. S1 in ESI†). However, due to abrupt expansion process, the residual impurities left on curled graphene, which are sulfides from the EDX (by TEM) results (Seen Fig. S2b in ESI†). The lower amounts of sulfides are not evidently, compared with the strong carbon peak. Subsequently, the treatment of HNO_3 for MG-IPA is similar as the purity of carbon materials.[47] After one-hour sonication in strong HNO_3, the clean multilayer graphene is displayed in Fig. 1d and Fig. S3a. In comparison with MG-IPA (Fig. S2b), the EDX results of MG-HNO_3 (Fig. S4b) exhibit that the amounts of sulfides have decreased, which indicates that the treatment of HNO_3 is efficient to clean the surface of multilayer graphene. Based on the Fig. S3d, the impurities of Cu and Si is from the TEM grid. As for the layers, multilayer graphene is consisted of 4-12 layers (Fig. 1d and Fig. S3b). Besides, in Fig. S3c, the monolayer sheet is exited at the edge of MG, which is determined using the selected area electron diffraction method. The six-fold symmetry of the diffraction pattern derives from the honeycomb structure of carbon atoms of the graphene. The intense hexagonal spots in the inner set of the diffraction pattern of Fig. S3d confirm the presence of monolayer graphene.[48] Interestingly, the EG can not be dispersed in the absolute ethanol and deionized water with the sonication due to its hydrophobic property. Herein, the solvent as the preferred choice to disperse graphene is oleophilic without the assistance of surfactant.

Raman spectroscopy is also a sensitive tool to probe the properties carbon materials. According to the primary features of graphene in the Raman spectra,[49] the D-band band is related with disorder-induced scattering resulting from imperfections or loss of hexagonal symmetry of disordered graphite; the G-band corresponds to an E_{2g} mode of graphite is associated with vibration of sp^2-bonded carbon atoms in a two-dimensional hexagonal lattice. Fig. 2 shows typical Raman spectra of worm-like EG, MG-IPA and MG-HNO_3, respectively. All three samples have the clear peaks of G-band at ca. 1586cm^{-1} and 2D-band at ca. 2756 cm^{-1}. However, the disorder-induced D peak (1372cm^{-1}) of the three samples was not evident in the Raman spectra. Hence, the preparation of high-quality and large-sheet multilayer graphene can be achieved via the simple process of rapid heat-treatment and the ultrasonic treatment in the IPA and HNO_3.

Similarly, in the previous reports, [34, 39, 40] the graphene is easily

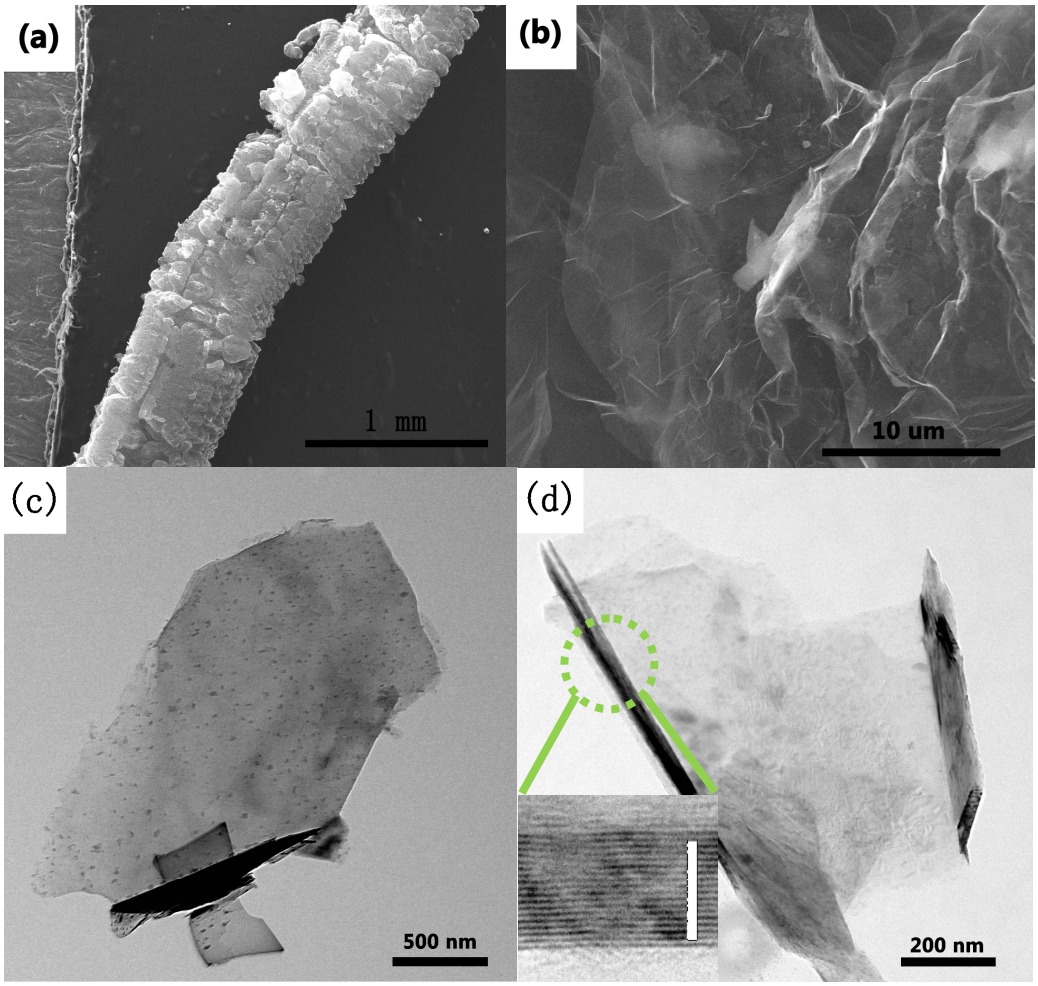

Fig. 1. SEM of worm-like EG (a and b), TEM of MG-IPA (c) and MG-HNO_3 (d), white bar is 5 nm.

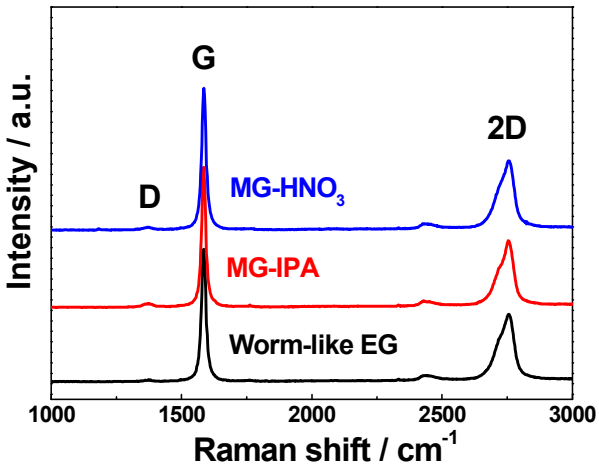

Fig. 2 . The Raman spectra of worm-like EG, MG-IPA, and MG-HNO_3.

dispersed in the NMP solvent and the supernatant liquid contain monolayer graphene via a simple sonication. Therefore, the facile strategy is designed to fabricate the composite electrode by utilizing the NMP solvent containing low concentration of MG (5 mg/mL). Next, SEM was again used to observe the composite electrode containing the MG sheets. As shown in Fig 3a and b, the translucent MG sheets are embedded inside composite electrode and thereby ambient C-LFP and AB particles are attached to the MG sheets. Besides, XRD patterns of four samples are shown in Fig. 3c. MG has a peak at 2θ=26.3 °C (d=0.339), the average interlayer distance is slightly increased compared to pure graphite (d=0.0335), which confirms this simple synthetic method of MG is efficient. The slurry containing 1 wt.% amount of MG is dried before XRD measurements. However, due to a low amount of MG in composite electrode as well as the impact from AB diffraction peaks, a bread peak at *ca.*26 °C is observed in the XRD patterns of C-LFP/MG as hybrid XRD patterns of AB and MG, compared with that of C-LFP. But the pattern at right side of the shape peak is a little stronger than one at left side. To some extent, the existence of MG is also identified in composite electrode and will be beneficial to greatly enhancing the electronic conductivity of whole bulk electrode.

The electrochemical test

The composite electrode (C-LFP/MG) and common electrode (C-LFP/AB) were assembled into coin cells to evaluate their electrochemical performance. The charge process is carried with constant current at different rate, followed by the constant voltage of 4.2 V for 10 minutes. When the charge/discharge process is investigated at the low rate of 1*C*, the potential voltage and capacity of C-LFP/MG is the almost same as that of C-LFP/AB due to the sufficient conductivity of acetylene black (as preferred choice of common conducting additives) in bulk electrode. The C-LFP/MG exhibits the discharge capacity of ca. 139.1 mAh·g^{-1}, a little more 2.8 % capacity than that of C-LFP/AB, and the operating flat voltage of ca. 3.4 V, nearly the theoretical value of $LiFePO_4$. However, the differences between the C-LFP/MG and C-LFP/AB are reflected evidently with increasing the rate. The C-LFP/MG exhibits higher operating flat voltage and capacity, compared with the deteriorated performance of C-LFP/AB. The discharge capacities of C-LFP/MG at 10*C* and 20*C* are 121.9 and 107.8 mAh·g^{-1}, respectively, which is enhanced by 5.4 % and 9.6 % due to the addition of the MG sheets. Even at the high-rate of 20*C*, the operating flat voltage of more than 3.0 V is still maintained obviously for near two minutes. The higher capacity and lower polarization indicate that the MG-modification for bulk electrode is efficient, leading to the optimization of electronic transport. Therefore, based on the merits of high current and high voltage, the power performance of bulk electrode ($P = U * I$) can meet the requirements of EVs and HEVs.

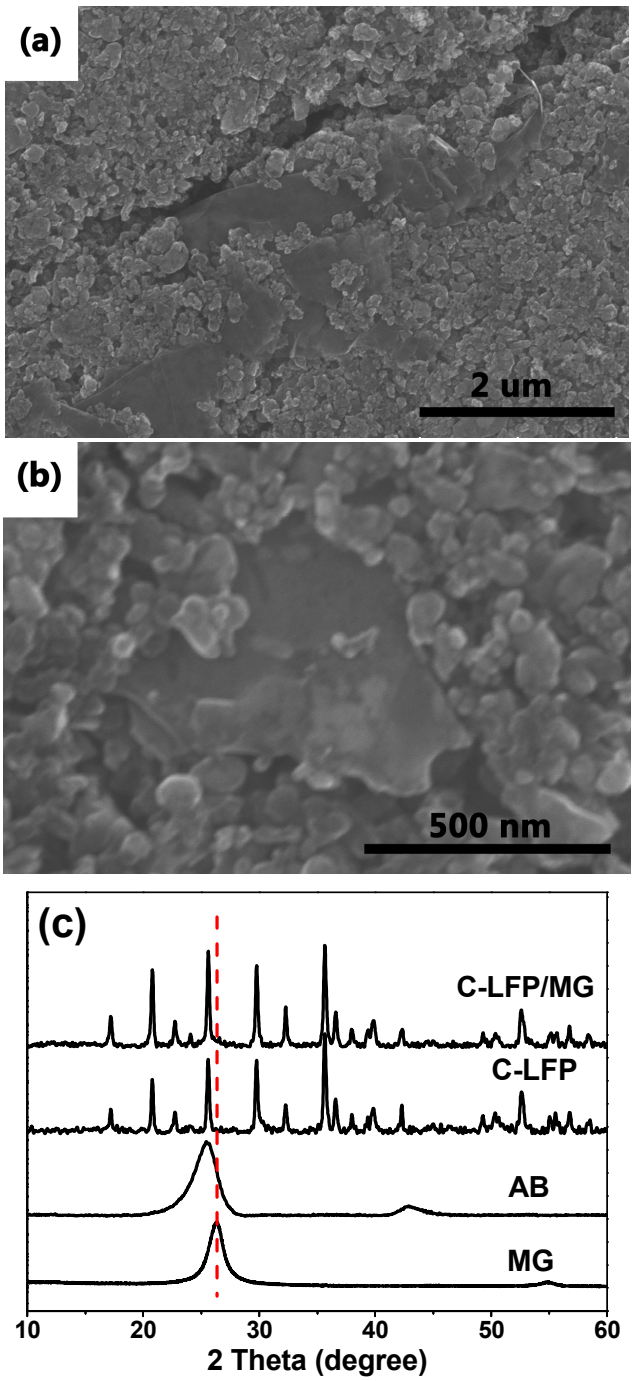

Fig. 3 SEM of the composite electrode (a and b) and XRD patterns of the different samples (c).

Subsequently, the cycling performance and stability were measured via the high-rate charge/discharge process. With the seven cycles activated at 1*C* rate, the discharge capacity of C-LFP/MG is maintained *ca.* 120 mAh·g^{-1} at 10*C* rate after more than 100 cycles. Due to excellent capacity retention of carbon-coated $LiFePO_4$ nanocomposites in our previous report[45, 46], the electronic conductive additive of MG for bulk electrode has not deteriorated the whole cycle performance, indicating that the attachment of active particles on the MG sheets is stability.

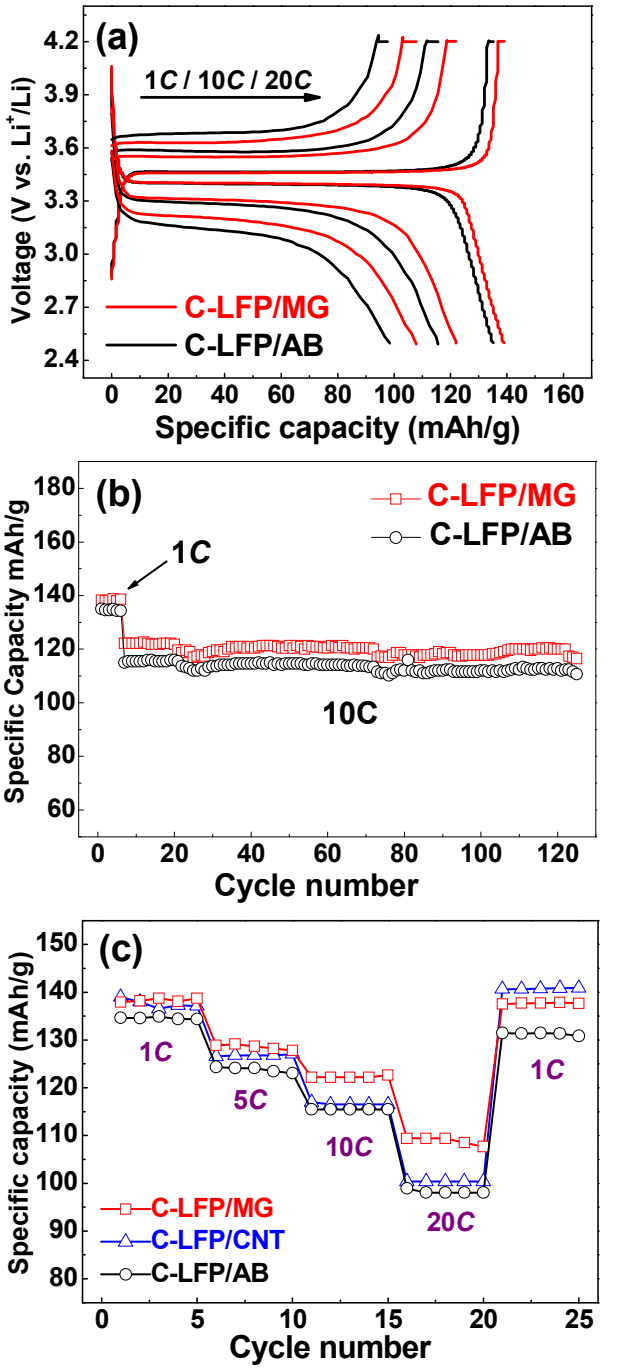

Fig. 4 The charge and discharge profiles of C-LFP/MG and C-LFP/AB at 1*C*, 10*C* and 20*C* rate (a) ; High-rate cycling performance of C-LFP/MG and C-LFP/AB (b); the discharge comparison of C-LFP/MG, C-LFP/CNT and C-LFP/AB at different rate(c).

Carbon nanotube (CNT) is often adopted as additives for preparation of $LiFePO_4$-based composites or bulk electrode.[50] The morphology of CNT is shown in Fig. S5. Due to superior conducive property of CNT, it is also regarded as ideal fast pathways for electronic transport in bulk electrode and thereby relative papers report evident improvements for the performance of electrode.[50] The $LiFePO_4$-based electrode also is modified with 1 wt.% CNT, denoted as C-LFP/CNT, and fabricated as the same craft as that of MG. In Fig. 4c, the composite electrode of C-LFP/CNT discharges similar capacity of 138.8 mAh·g^{-1} at 1*C* rate as that of C-LFP/MG and C-LFP/AB. At the high rate of 20*C*, the discharge capacity of C-LFP/CNT is lower than that of C-LFP/MG, but it is still a little better than that of C-LFP/AB. As for this possible reason, the limiting particles can be attached to the CNT in bulk electrode, which are fewer than that of MG, due to the morphology of CNT with large length/width ratio. After the great improvement of $LiFePO_4$-based active nanograins, this result from bulk electrode is different from an evident improvement for composite particles with CNT-modification.[51] Importantly, considered with cost and synthetic process, such multilayer graphene is an optimal choice as the conductive additives.

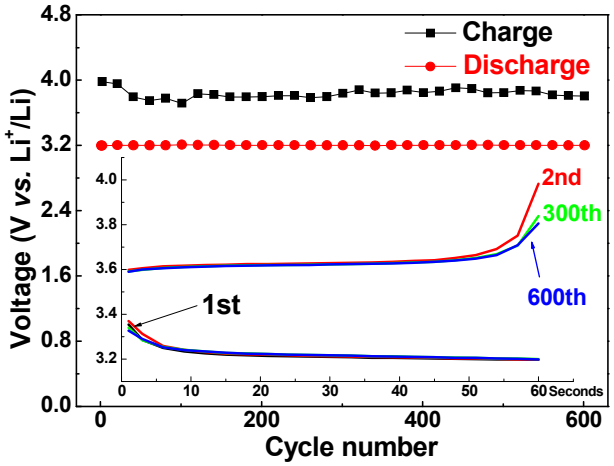

Fig. 5 The pulse performance of C-LFP/MG and C-LFP/AB with 60-second rapid charge/discharge process (c) , the inset image is the operating voltage profiles of rapid charge/discharge process for one minute at 10*C* rate.

The property of pulse performance is evaluated with 60-second rapid charge/discharge process, which simulates the starting or accelerating and braking of EVs and HEVs in urban congestion. Initially, the electrode of C-LFP/MG is fully charged at 1*C* rate and then under constant voltage of 4.2 V for 10 minutes. This rapid charge/discharge process starts with galvanostatic discharge for 60s at 10*C* and cycles with 600 times. Fig. 5 records the terminal operating voltage of charge and discharge process. Despite the fluctuation of terminal charge voltage from 3.6 V to 3.8 V, the terminal discharge voltage is stable at ca. 3.2 V with cycle numbers. The inset image of Fig. 5 shows that the operating voltage varies with the time during 60 seconds. The smooth curve of discharge exhibits a stable voltage output, which is beneficial to the stability of battery system. Therefore, it illustrates the capability of electronic conducting is enhanced in composite electrode.

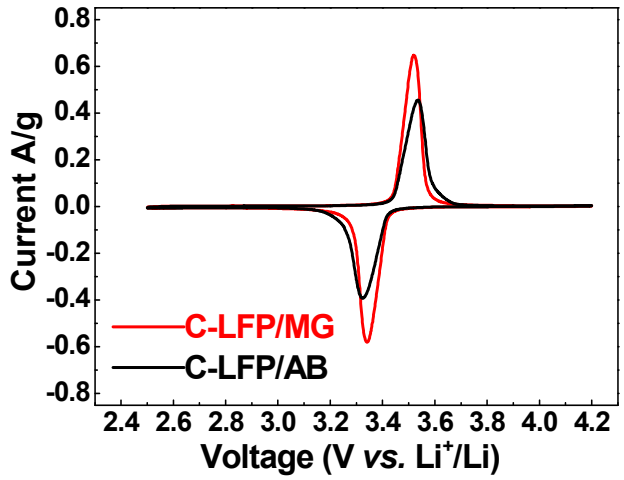

Fig. 6. The CV curves of LFP-G and LFP, scan rate 0.1 mVs^{-1};

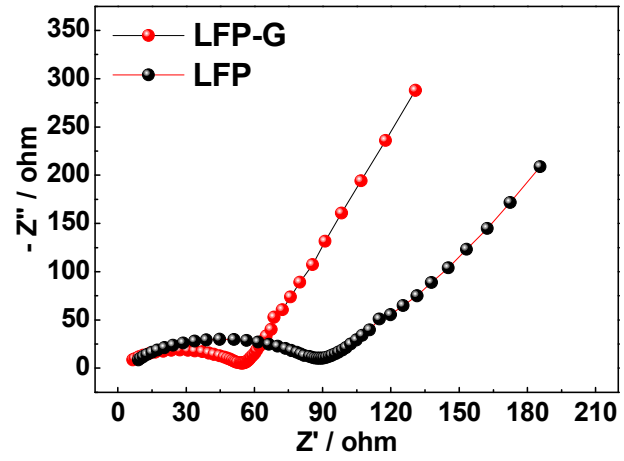

Fig. 7. The Nyquist plots of LFP-G and LFP.

In order to explain excellent power performance of C-LFP/MG, the cyclic voltammetry and electrochemical impedance spectroscopy are used to investigate the C-LFP/MG and C-LFP/AB. As shown in the CV test of Fig. 6, the C-LFP/MG shows the reduced potential interval between two anodic/cathodic peaks is 0.18 V. By contrast, this interval for C-LFP/AB is 0.29 V. Besides, the current of peaks for C-LFP/MG also is higher than that of C-LFP/AB. Such distinctions indicate that the internal resistance of bulk electrode is reduced, which can be ascribed to the large-size MG sheets, assisting electrons in arriving at C-LFP active particles. Subsequently, the EIS spectra of C-LFP/MG and C-LFP/AB continue to be collected after full charge of as-prepared electrode with the diameter of 14 mm. As shown in Fig. 7, the EIS spectra is composed of a quasisemicircle at the range from high to middle frequency and a straight slopping line at the low frequency range. The intercept in high frequency region is related to the ohmic series resistance (R_U), including interparticle contact resistance, electrolyte resistance and other physical resistances. Based on the same assembled craft of coin cells, the R_U of C-LFP/MG is only 6.5 ohm, which is lower than R_U of LFP (9.1 ohm). The reduced R_U probably arises from the contribution of superior conductivity of graphene. Besides, the size of carbon-coated $LiFePO_4$ particles has been reduced to the nano scale via advanced synthesis, resulting in better electrical conductivity and enhanced charge transfer. Combining with the contribution of MG on bulk electrode, the semicircle of C-LFP/MG with a much smaller diameter is obtained. From a series of above tests, the excellent power performance is to some extent attributed to the optimal pathways of electronic transport inside bulk electrode after the modification with multilayer graphene. It could be rationally concluded as followed analysis. As for the common electrode, the active materials, acetylene black and insulated PVdF binder are mixed uniformly and pasted on the Al foils. Therefore, the active particles are surrounded with conductive grains, which carry electrons and alleviate the change of volume during the charge/discharge process. Therefore, the C-LFP

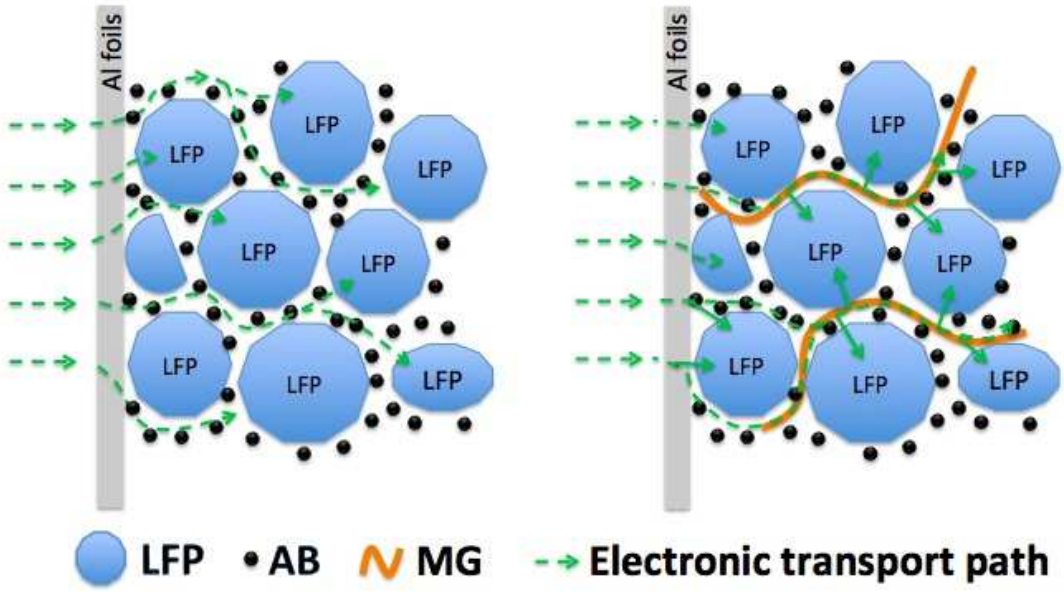

Fig. 7. The general view on the path of electronic transport between the composite electrode and common electrode.

particle get elecrons from their ambient AB particles. However, such conductive system of electronic transport based on the intimate contact among the particles, just like the "Kangaroo jump", causes the increasing internal resistance. When the pulse current charge/discharge process takes place, namely, physical resistance of outer electrode is higher than that of inner electrode near the current collector. As a result, the instantaneous current is uneven in bulk electrode, leading to the polarization. In contrast, there are double conductive additives to improve the electronic kinetics of the composite electrode. The acetylene black and multilayer graphene play an important but different role on enhancing the electrochemical properties of the $LiFePO_4$ material. In addition to the above function of acetylene black as same as the common electrode, the major contribution of large-size multilayer graphene is to establish fast pathways of far conducting electrons from the current collector to the outer electrode. The electrons easily arrive at outer active materials along the graphene sheets and acetylene black particles. The pathways of electronic migration is shown in Fig. 9. The enhanced conductivity of the whole electrode accelerates synchronous charge/discharge process inside bulk electrode due to the outer active materials attaching to the graphene. The higher operating flat voltage is maintained in period of several minutes, which is beneficial to ensuring the stable voltage of whole battery system. Besides, the consistency of batteries is also, to some extent, enhanced at different rate. Therefore, the improved electronic conductivity of bulk electrode arising from the modification of MG sheets is responsible for the excellent power performance.

Conclusions

The MG sheets as conductive additive enhance the conductivity of whole $LiFePO_4$-based electrode. Both higher discharge current and higher operating flat voltage are a sign of the great power performance of bulk electrode. Besides, the pulse performance and cycling stability can meet the stringent requirements of EVs and HEVs. The optimized paths for electronic transport in bulk electrode are responsible for the enhancement of high-rate performance in LIBs. Therefore, such modification for bulk electrode with multilayer graphene is simple and efficient. Moreover, in the view of the ease of fabrication with decorating bulk electrode with graphene, this facile and economical strategy ensures a controlled cost of cathode composite materials for the popularization of LIBs.

Acknowledgement

We appreciate the support of National Natural Science Foundation of China (No. 50974045).

Notes and references

Harbin Institute of Technology, School of Chemical Engineering and Technology, Xidazhi Street, 150001 Harbin, China.Fax:86 451 86413721; Tel: 86 451 86413751; E-mail: wangdianlongwbhit@163.com

†Electronic Supplementary Information (ESI) available: [details of any supplementary information available should be included here]. See DOI: 10.1039/b000000x/

1. A. K. Padhi, *J. Electrochem. Soc.*, 1997, **144**, 1188.
2. D. Jugović and D. Uskoković, *J. Power Sources*, 2009, **190**, 538.
3. L.-X. Yuan, Z.-H. Wang, W.-X. Zhang, X.-L. Hu, J.-T. Chen, Y.-H. Huang and J. B. Goodenough, *Energy Environ. Sci.*, 2011, **4**, 269.
4. A. Yamada, M. Hosoya, S.-C. Chung, Y. Kudo, K. Hinokuma, K.-Y. Liu and Y. Nishi, *J. Power Sources*, 2003, **119–121**, 232.
5. Y. Zhang, Q.-y. Huo, P.-p. Du, L.-z. Wang, A.-q. Zhang, Y.-h. Song, Y. Lv and G.-y. Li, *Synth. Met.*, 2012, **162**, 1315.
6. Z. Chen and J. R. Dahn, *J. Electrochem. Soc.*, 2002, **149**, A1184.
7. H. Ni, J. Liu and L.-Z. Fan, *Nanoscale*, 2013, **5**, 2164.
8. J. Zhao, J. He, J. Zhou, Y. Guo, T. Wang, S. Wu, X. Ding, R. Huang and H. Xue, *J. Phys. Chem. C*, 2011, **115**, 2888.
9. K. S. Park, J. T. Son, H. T. Chung, S. J. Kim, C. H. Lee, K. T. Kang and H. G. Kim, *Solid State Commun.*, 2004, **129**, 311.
10. J. Wang and X. Sun, *Energy Environ. Sci.*, 2012, **5**, 5163.
11. S.-Y. Chung, J. T. Bloking and Y.-M. Chiang, *Nat Mater.*, 2002, **1**, 123.
12. M. Wagemaker, B. L. Ellis, D. Lützenkirchen-Hecht, F. M. Mulder and L. F. Nazar, *Chem. Mater.*, 2008, **20**, 6313.
13. C. Ban, W.-J. Yin, H. Tang, S.-H. Wei, Y. Yan and A. C. Dillon, *Adv. Energy Mater.*, 2012, **2**, 1028.
14. S. Ferrari, R. L. Lavall, D. Capsoni, E. Quartarone, A. Magistris, P. Mustarelli and P. Canton, *J. Phys. Chem. C*, 2010, **114**, 12598.
15. M. K. Devaraju and I. Honma, *Adv. Energy Mater.*, 2012, **2**, 284.
16. A. Yamada, S. C. Chung and K. Hinokuma *J. Electrochem. Soc.*, 2001, **148**, A224.
17. M. Wang, Y. Yang and Y. Zhang, *Nanoscale*, 2011, **3**, 4434.
18. K. I. Bolotin, K. J. Sikes, Z. Jiang, M. Klima, G. Fudenberg, J. Hone, P. Kim and H. L. Stormer, *Solid State Commun.*, 2008, **146**, 351.
19. S. W. Oh, Z.-D. Huang, B. Zhang, Y. Yu, Y.-B. He and J.-K. Kim, *J. Mater. Chem.*, 2012, **22**, 17215.
20. Y. Ding, Y. Jiang, F. Xu, J. Yin, H. Ren, Q. Zhuo, Z. Long and P. Zhang, *Electrochem. Commun.*, 2010, **12**, 10.
21. Y. Shi, S.-L. Chou, J.-Z. Wang, D. Wexler, H.-J. Li, H.-K. Liu and Y. Wu, *J. Mater. Chem.*, 2012, **22**, 16465.
22. X. Zhou, F. Wang, Y. Zhu and Z. Liu, *J. Mater. Chem.*, 2011, **21**, 3353.
23. B. Wang, D. Wang, Q. Wang, T. Liu, C. Guo and X. Zhao, *J. Mater. Chem. A*, 2013, **1**, 135.
24. Y. Wu, Z. Wen, H. Feng and J. Li, *Chem. Europ. J.*, 2013, **19**, 5631.
25. C. Su, X. Bu, L. Xu, J. Liu and C. Zhang, *Electrochimica Acta*, 2012, **64**, 190.
26. J. Yang, J. Wang, Y. Tang, D. Wang, X. Li, Y. Hu, R. Li, G. Liang, T.-K. Sham and X. Sun, *Energy Environ. Sci.*, 2013, **6**, 1521.
27. Y. Zhang, W. Wang, P. Li, Y. Fu and X. Ma, *J. Power Sources*, 2012, **210**, 47.
28. J. Yang, J. Wang, D. Wang, X. Li, D. Geng, G. Liang, M. Gauthier, R. Li and X. Sun, *J. Power Sources*, 2012, **208**, 340.
29. L.-H. Hu, F.-Y. Wu, C.-T. Lin, A. N. Khlobystov and L.-J. Li, *Nat. Commun.*, 2013, **4**.
30. Z. Feng, C. Zhang, J. Chen, Y. Wang, X. Jin, R. Zhang and J. Hu, *Rsc Advances*, 2013, **3**, 4408.
31. J. Ha, S.-K. Park, S.-H. Yu, A. Jin, B. Jang, S. Bong, I. Kim, Y.-E. Sung and Y. Piao, *Nanoscale*, 2013, **5**, 8647.
32. H. Bi, F. Huang, Y. Tang, Z. Liu, T. Lin, J. Chen and W. Zhao, *Electrochim. Acta*, 2013, **88**, 414.
33. Y. Tang, F. Huang, H. Bi, Z. Liu and D. Wan, *J. Power Sources*, 2012, **203**, 130.
34. F.-Y. Su, Y.-B. He, B. Li, X.-C. Chen, C.-H. You, W. Wei, W. Lv, Q.-H. Yang and F. Kang, *Nano Energy*, 2012, **1**, 429.
35. L. Wang, L.-H. Tian, G.-D. Wei, F.-M. Gao, J.-J. Zheng and W.-Y. Yang, *J. Inorg. Mater.*, 2011, **26**, 1009.
36. W. Yang, G. Chen, Z. Shi, C.-C. Liu, L. Zhang, G. Xie, M. Cheng, D. Wang, R. Yang, D. Shi, K. Watanabe, T. Taniguchi, Y. Yao, Y. Zhang and G. Zhang, *Nat. Mater.*, 2013, **12**, 792.
37. A. Bagri, C. Mattevi, M. Acik, Y. J. Chabal, M. Chhowalla and V. B. Shenoy, *Nat Chem*, 2010, **2**, 581.
38. D. P. Singh, F. M. Mulder, A. M. Abdelkader and M. Wagemaker, *Adv. Energy Mater.*, 2013, **3**, 572.
39. X. Fu, X. Song and Y. Zhang, *Mater. Letters*, 2012, **70**, 181.
40. W. Gu, W. Zhang, X. Li, H. Zhu, J. Wei, Z. Li, Q. Shu, C. Wang, K. Wang, W. Shen, F. Kang and D. Wu, *J. Mater. Chem.*, 2009, **19**, 3367.

41. S. R. Dhakate, N. Chauhan, S. Sharma, J. Tawale, S. Singh, P. D. Sahare and R. B. Mathur, *Carbon*, 2011, **49**, 1946.
42. L. Zhu, X. Zhao, Y. Li, X. Yu, C. Li and Q. Zhang, *Mater. Chem. Phys.*, 2013, **137**, 984.
43. M. Quintana, M. Grzelczak, K. Spyrou, B. Kooi, S. Bals, G. Van Tendeloo, P. Rudolf and M. Prato, *Chem Commun.*, 2012, **48**, 12159.
44. C. Liu, G. Hu and H. Gao, *The J. Supercritical Fluids*, 2012, **63**, 99.
45. Q. Wang, D. Wang and B. Wang, *Ionics*, 2012.
46. B. Wang, B. H. Xu, T. Liu, P. Liu, C. Guo, S. Wang, Q. Wang, D. Wang and G. Zhao, *Nanoscale*, 2013.
47. B. Y. Venhryn, Z. A. Stotsko, I. I. Grygorchak, B. P. Bakhmatyuk and S. I. Mudry, *Ultrasonics SonoChem.*, 2013, **20**, 1302.
48. Y. Hernandez, V. Nicolosi, M. Lotya, F. M. Blighe, Z. Sun, S. De, I. T. McGovern, B. Holland, M. Byrne, Y. K. Gun'Ko, J. J. Boland, P. Niraj, G. Duesberg, S. Krishnamurthy, R. Goodhue, J. Hutchison, V. Scardaci, A. C. Ferrari and J. N. Coleman, *Nat Nano*, 2008, **3**, 563.
49. L. M. Malard, M. A. Pimenta, G. Dresselhaus and M. S. Dresselhaus, *Phys. Rep.*, 2009, **473**, 51.
50. X.-M. Liu, Z. d. Huang, S. w. Oh, B. Zhang, P.-C. Ma, M. M. F. Yuen and J.-K. Kim, *Compos. Sci. Technol.*, 2012, **72**, 121.
51. M. Chen, C. Du, B. Song, K. Xiong, G. Yin, P. Zuo and X. Cheng, *J. Power Sources*, 2013, **223**, 100.